

Two-photon absorption of styryl-quinolinium, -pyridinium, and -barbituric acid derivatives, and intramolecular charge transfer

XiaoMei Wang, Chun Wang, WenTao Yu, YuFang Zhou, Xian Zhao, Qi Fang, and MinHua Jiang

Abstract: A series of new chromophores, styryl-parent end-capped with various donors, and with barbituric acid, methyl-pyridinium, and methyl-quinolinium as the acceptors, have been synthesized and characterized by element analysis or X-ray diffraction. Using the Z-scan system, their two-photon absorption (TPA) cross-section values (δ) have been determined under excitation with 10 Hz, and 1064 nm, 35 ps mode-locked Nd:YAG laser pulse in DMF with $d_0 = 0.05$ M. The effective δ value is as high as 10.9×10^{-48} cm⁴ s per photon for *trans*-4-(4'-*N,N*-diphenyl amino) styryl-*N*-methyl quinolinium iodide (DPASQI). The δ value increases from barbituric acid- to pyridinium- to quinolinium-derivatives apparently due to the increase in both the conjugated degree and planarity; however, when the acceptor is fixed, the δ value increases from dialkyl amino groups to diphenyl amino groups even though the latter is a weaker donor than the dialkyl amino groups. Theoretical calculations confirm that the increased distortion from planarity for the barbituric acid derivative makes its δ value decrease. The relatively large δ value for quinolinium- or pyridinium-derivatives originates from larger intramolecular charge transfer, which can be characterized by the difference of dipole moment ($\Delta\mu_{ge}$) between the S_0 and S_1 , and the transition dipole moment ($M_{ee'}$) between S_1 and S_2 .

Key words: two-photon absorption, intramolecular charge transfer, styryl-quinolinium, styryl-pyridinium, styryl-barbituric acid.

Résumé : On a synthétisé une série de nouveaux chromophores, un styryle de base recouvert de divers donneurs et des accepteurs comme l'acide barbiturique et les ions méthylpyridinium et méthylquinoléinium et on les a caractérisés par analyse élémentaire ou diffraction des rayons X. Faisant appel à un système à balayage Z et opérant dans le DMF avec d_0 0,05 M, une excitation de 10-Hz et une pulsation laser Nd:YAG de 35 ps en mode bloqué, on a déterminé les valeurs, δ , des sections efficaces de leur absorption de deux photons. Dans le cas de l'iodure du *trans*-4-(4'-*N,N*-diphénylamino) styryl-*N*-méthylquinoléinium (« DPASQI »), la valeur δ effective s'élève jusqu'à $10,9 \times 10^{-48}$ cm⁴ s/photon. Par ailleurs, la valeur de δ augmente en passant de l'acide barbiturique, puis aux dérivés pyridinium et quinoléinium; il semble que cette situation résulte d'une augmentation tant du degré de conjugaison que de la planarité. De plus, lorsque l'accepteur est fixé, la valeur de δ augmente des groupes dialkylamino aux groupes diphénylamino même si ces derniers sont des donneurs plus faibles que les groupes dialkylamino. Des calculs théoriques confirment que, dans le cas de l'acide barbiturique, l'augmentation de la distorsion par rapport à la planarité provoque une diminution de la valeur de δ . La valeur relativement élevée de δ pour les dérivés quinoléinium et pyridinium trouverait son origine dans un important transfert de charge intramoléculaire qui peut être caractérisé par la différence du moment dipolaire ($\Delta\mu_{ge}$) entre S_0 et S_1 et la transition du moment dipolaire ($M_{ee'}$) entre S_1 et S_2 .

Mots clés : absorption à deux photons, transfert de charge intramoléculaire, styryl-quinoléinium, styryl-pyridinium, styryl-acide barbiturique.

[Traduit par la Rédaction]

Introduction

Organic conjugated chromophores with a large two-photon absorption (TPA) cross-section emerge as very attractive elements for use in a number of optical applications such as op-

tical data storage, up-converted lasing, and optical power limiting (1–10). Numerous organic compounds have been investigated experimentally and theoretically in order to understand the structure–property relationship of materials with large TPA cross-sections (11–17). Some general structural parameters for increasing the molecular TPA cross-section values (δ) have gradually been drawn in several laboratories (11–15). For example: (i) increasing the donor and acceptor strength; (ii) changing the character of the conjugated bridge; (iii) increasing the planarity of the chromophores; and (iv) extending the conjugated length. The results of theoretic-

Received June 19, 2000. Published on the NRC Research Press Web site on March 14, 2001.

X.M. Wang, C. Wang, W.T. Yu, Y.F. Zhou, X. Zhao, Q. Fang, and M.H. Jiang.¹ State Key Laboratory of Crystal Materials, Shandong University Jinan, 250100 China.

¹Corresponding author (e-mail: mhjiang@sdu.edu.cn).

Table 1. Optical properties and calculated structural parameters for all chromophores.

Chromophore	$\theta^{d/o a}$	$\Delta\mu_{ge}$ (debye)	$M_{ee'}$ (debye)	β (cm GW ⁻¹)	δ ($\times 10^{-48}$) cm ⁴ s photon ⁻¹
HMASBA	70	0.7	—	0.60	3.9
PSPI	Planar	3.4	8.5	0.91	5.7
DEASPI	Planar	8.1	8.2	1.09	6.8
HEASPI	Planar	8.2	8.6	1.12	7.0
DPASPI	Planar	11.8	9.8	1.42	8.8
HMASQI	Planar	10.6	—	1.41	8.8
DPASQI	Planar	12.1	—	1.75	10.9

^aThe dihedral angle between two rings of the backbone.

Table 2. Crystallographic data for DPASPI and HMASQI.

	DPASPI	HMASQI
Formula	C ₂₆ H ₂₃ IN ₂	C ₂₁ H ₂₃ IN ₂ O
MW	490.36	446.31
<i>T</i> (K)	293	293
System	Orthorhombic	Monoclinic
Space group	<i>Pbca</i>	<i>P2₁/n</i>
<i>a</i> , <i>b</i> , <i>c</i> (Å)	10.5638(14), 11.1909(19), 37.255(4)	10.0512(11), 16.2879(12), 12.3328(8)
α , β , γ (°)	90	90, 102.307(6), 90
<i>V</i> (Å ³)	4404.2(11)	1972.6(3)
<i>Z</i>	8	4
<i>D</i> calcd. (g cm ⁻³)	1.479	1.503
Absorption coefficient (mm ⁻¹)	1.468	1.634
<i>F</i> (000)	1968	896
Crystal size (mm)	0.20 × 0.28 × 0.25	0.35 × 0.30 × 0.20
θ range (deg)	2.2–25.0	2.10–26.00
Index range	−12 ≤ <i>h</i> ≤ 1, −13 ≤ <i>k</i> ≤ 1, −44 ≤ <i>l</i> ≤ 1	−1 ≤ <i>h</i> ≤ 12, −1 ≤ <i>k</i> ≤ 20, −15 ≤ <i>l</i> ≤ 15
Refl. collected	4906	4906
Independent refl.	3847 [<i>R</i> (int) = 0.064]	3882 [<i>R</i> (int) = 0.0230]
Max and min transmission	0.301 and 0.202	0.689 and 0.561
Final <i>R</i> indices [<i>I</i> > 2σ(<i>I</i>)]	<i>R</i> ₁ = 0.0776, <i>wR</i> ₂ = 0.2372	<i>R</i> ₁ = 0.0358, <i>wR</i> ₂ = 0.0824
<i>R</i> indices	<i>R</i> ₁ = 0.1409, <i>wR</i> ₂ = 0.2372	<i>R</i> ₁ = 0.0558, <i>wR</i> ₂ = 0.0939
Largest diff. peak and hole (e Å ⁻³)	1.79 and −1.11	0.5809 and −0.499
GoF on <i>F</i> ²	0.93	1.066
Data/restraint/parameters	3847 / 0 / 262	3882 / 0 / 226

cal studies further reveal that the TPA δ value is related to the imaginary part of the third-order polarizability (16),

$$[1] \quad \delta(\omega) = \frac{4\pi h\omega^2}{n^2 c^2} L^4 \text{Im } \gamma(-\omega; \omega, \omega, -\omega)$$

where *h* is Planck's constant, *n* is the index of refraction of the medium, *L* is a local field factor (equal to 1 for vacuum), and *c* or ω is the speed of light or the frequency of light. When the frequency (ω) is left out of consideration, the third-order polarizability (γ) can be expressed as eq. [2] (17–18),

$$[2] \quad \gamma_{xxxx} = 24 \frac{M_{ge}^2}{E_{ge}^2} \left[\frac{\Delta\mu_{ge}^2}{E_{ge}} + \sum_{e'} \frac{M_{ee'}^2}{E_{ge'}} - \frac{M_{ge}^2}{E_{ge}} \right]$$

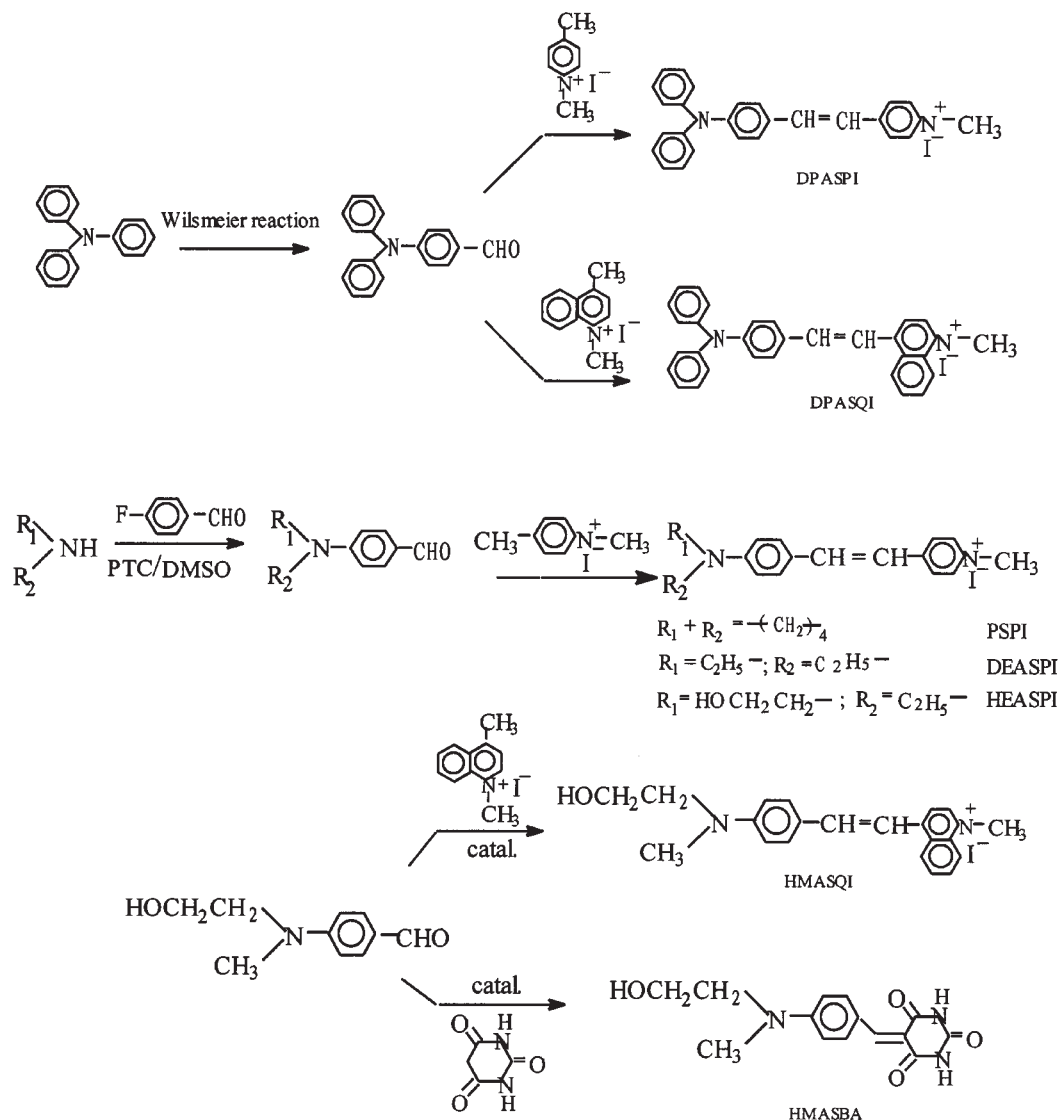
where $\Delta\mu_{ge}$ is the difference of dipole moment between the ground state (*S*₀) and the first excited state (*S*₁); *M*_{ge} or *M*_{ee'} is the transition dipole moment between *S*₀ and *S*₁ or between the two lowest excited states, that is, *S*₁ and *S*₂, and *E*_{ge} or *E*_{ge'} is the difference between ground and excited state energy or

between the two excited states. The first two terms in eq. [2] make a positive contribution to the TPA process (17).

It is evident that the TPA δ value is dependent not only on the difference between the ground- and excited-state dipole moment but also the transition dipole moment between two excited states. It is rational to deduce that materials with large $\Delta\mu_{ge}$ and *M*_{ee'} must have exhibited high δ values due to stronger intramolecular charge transfer.

Based on this idea, we calculated structural parameters, such as $\Delta\mu_{ge}$ and *M*_{ee'}, for π -donor–acceptor compounds. One of the better candidate groups for generating a larger intramolecular charge shift is the substituted styryl-pyridinium cations. Other promising candidates are the substituted styryl-quinolinium cations. These kinds of salts possess the fused aromatic heterocyclic ring that may improve π -electron delocalization and result in better TPA properties. In addition the structural parameters for the barbituric acid derivative have also been calculated to examine the influence planarity and conjugated length upon TPA property. The calculation results are shown in Table 1.

Scheme 1.



methyl-pyridinium and further to methyl-quinolinium moiety, and also by varying the donor strengths in the order of: dialkylamino group > diphenylamino group. On the basis of correlated quantum-chemical calculation and experimental measurement results, we further demonstrate that large $\Delta\mu_{ge}$ and $M_{e\sigma}$ can result in large intramolecular charge transfers, which have contributed to enhance the two-photon absorption cross-section.

Experimental

Synthesis

The decomposition temperatures were measured on a Perkin–Elmer TGS-2 thermogravimetric analyzer at a rate of 20°C min⁻¹ under nitrogen atmosphere. Element analyses were performed on a Perkin 2400. Mass spectra were recorded with an HP5989 apparatus. NMR spectra were determined on FX-90Q NMR spectrometer (TMS as standard).

Synthesis of donor and acceptor components

4-Pyrrolidinyl benzaldehyde, 4-(*N,N*-diethyl amino)benzaldehyde, 4-(*N,N*-diphenyl amino)benzaldehyde, 4-(*N*-hydroxy-

ethyl-*N*-ethyl amino)benzaldehyde and 4-(*N*-hydroxyethyl-*N*-methyl amino)benzaldehyde were synthesized according to ref. 11.

4-Methyl-*N*-methylquinolinium iodide was synthesized by the reaction of lepidine (4.3 g, 30 mmol) and methyl iodide (4.4 g, 31 mmol) in ethanol (30 mL) at reflux temperature for 2 h. After cooling, the solution was filtered and recrystallized in ethanol. Yellow needle crystals were obtained with yield 80%.

Synthesis of chromophores

Chromophores were synthesized by the Knoevenagel condensation reaction of the appropriate substituted benzaldehyde and the acceptor components such as 4-methyl-*N*-methylpyridinium iodide and 4-methyl-*N*-methylquinolinium iodide with a catalytic amount of piperidine. For example, a mixture of equal molar 4-(*N,N*-diphenyl amino)benzaldehyde (3.5 g, 13 mmol) and 4-methyl-*N*-methylquinolinium iodide (3.7 g, 13 mmol) were stirred in ethanol (20 mL) at reflux temperature overnight in the presence of 4–5 drops piperidine. After cooling, the crude product of DPASQI

Table 3. Selected bond lengths (Å) and angles (°) for HMASQI.

N(1)—C(10)	1.331(5)	C(2)—C(3)	1.406(6)	C(9)—C(10)	1.372(6)
N(1)—C(2)	1.381(5)	C(3)—C(4)	1.355(6)	C(11)—C(12)	1.352(5)
N(1)—C(1)	1.475(5)	C(4)—C(5)	1.402(7)	C(12)—C(13)	1.442(5)
N(2)—C(16)	1.353(5)	C(5)—C(6)	1.367(6)	C(13)—C(18)	1.395(5)
N(2)—C(21)	1.464(6)	C(6)—C(7)	1.414(5)	C(13)—C(14)	1.403(5)
N(2)—C(19)	1.480(6)	C(7)—C(8)	1.448(5)	C(14)—C(15)	1.362(6)
O(1)—C(20)	1.465(6)	C(8)—C(9)	1.386(5)	C(15)—C(16)	1.408(6)
C(2)—C(7)	1.413(5)	C(8)—C(11)	1.436(5)	C(16)—C(17)	1.405(6)
C(17)—C(18)	1.379(6)	C(19)—C(20)	1.460(7)		
C(2)—N(1)—C(10)	120.5(3)	C(3)—C(4)—C(5)	120.4(4)	C(19)—C(20)—O(1)	105.4(4)
C(10)—N(1)—C(1)	118.9(4)	C(6)—C(5)—C(4)	120.1(4)	C(12)—C(11)—C(8)	124.9(4)
C(2)—N(1)—C(1)	120.6(3)	C(5)—C(6)—C(7)	121.4(4)	C(11)—C(12)—C(13)	126.4(4)
C(16)—N(2)—C(21)	121.6(4)	C(2)—C(7)—C(6)	117.3(4)	C(18)—C(13)—C(14)	115.9(4)
C(16)—N(2)—C(19)	121.9(4)	C(2)—C(7)—C(8)	120.3(3)	C(18)—C(13)—C(12)	123.6(3)
C(21)—N(2)—C(19)	115.6(4)	C(6)—C(7)—C(8)	122.4(4)	C(14)—C(13)—C(12)	120.4(4)
N(1)—C(2)—C(3)	120.4(4)	C(9)—C(8)—C(11)	122.9(4)	C(15)—C(14)—C(13)	122.0(4)
N(1)—C(2)—C(7)	119.2(3)	C(9)—C(8)—C(7)	115.9(3)	C(14)—C(15)—C(16)	122.3(4)
C(3)—C(2)—C(7)	120.4(4)	C(11)—C(8)—C(7)	121.3(3)	N(2)—C(16)—C(17)	120.5(4)
C(4)—C(3)—C(2)	120.4(4)	C(10)—C(9)—C(8)	121.9(4)	N(2)—C(16)—C(15)	123.5(4)
C(18)—C(17)—(16)	121.1(4)	N(1)—C(10)—C(9)	122.3(4)	C(17)—C(16)—C(15)	116.0(4)
C(17)—C(16)—(13)	122.6(4)	N(1)—C(10)—C(9)	122.3(4)	C(20)—C(19)—N(2)	109.9(4)

(*trans*-4-[(4'-*N,N*-diphenyl amino) styryl]-*N*-methyl quinolinium iodide) was filtered then purified by column chromatography on silica gel using acetone–ethanol (1:1) as the eluent. Needle deep-rose crystals were obtained after evaporation with a yield of 55% and the decomposition temperature (*T*_d) = 254.87°C. Element analysis: Anal. calcd.: C 66.67, H 4.66, N 5.18; found: C 66.03, H 4.59, N 5.12.

trans-4-[(4'-*N*-Hydroxyethyl-*N*-methyl amino) styryl]-*N*'-methyl quinolinium iodide (HMASQI) was synthesized by the same method. Purified by column chromatography on silica gel using acetonitrile–water (1:1) as the eluent. Strip-like purple crystals were obtained after evaporation. Yield 60% and *T*_d = 278.11°C. Element analysis: Anal. calcd.: C 56.51, H 5.19, N 6.28; found: C 56.48, H 5.13, N 6.38. (See Table 3 for bond lengths and angles).

Using the same method mentioned above, we synthesized the chromophores of pyridinium derivatives.

trans-4-[4'-(*N,N*-Diphenylamino) styryl]-*N*-methyl pyridinium iodide (DPASPI): The crude product was purified by column chromatography on silica gel using ethane–chloroform (1:1) as the eluent. Yield 82% and *T*_d = 260.2°C. Element analysis: Anal. calcd.: C 63.68, H 4.73, N 5.71; found: C 63.63, H 4.85, N 5.67. See Table 4 for bond lengths and angles.

trans-4-(4'-Pyrrolidinyl styryl)-*N*-methyl pyridinium iodide (PSPI): The crude product was purified by column chromatography on silica gel with ethanol as the eluent. Yield 82% and *T*_d = 260.6°C. Element analysis: Anal. calcd.: C 55.11, H 5.35, N 7.14; found: C 55.0, H 4.84, N 7.59.

trans-4-[4'-(*N,N*-Diethylamino) styryl]-*N*-methyl pyridinium iodide (DEASPI): Purified by column chromatography on silica gel with ethanol as the eluent. Yield 84% and *T*_d = 264.7°C. Element analysis: Anal. calcd.: C 54.84, H 5.88, N 7.10; found: C 54.34, H 5.46, N 6.98.

trans-4-[4'-(*N*-Hydroxyethyl-*N*-ethyl amino)styryl]-*N*-methyl pyridinium iodide (HEASPI): Purified by column chromatography on silica gel with ethanol as the eluent. Yield 85% and *T*_d = 286.7°C. Element analysis: Anal. calcd.: C 52.69, H 5.69, N 6.83; found: C 52.43, H 5.21, N 6.45.

5-(4-*N*-Hydroxyethyl-*N*-methylamino tyryl) barbituric acid (HMASBA): A mixture of equal molar 4-(*N*-hydroxyethyl-*N*-methyl amino) benzaldehyde (3.58 g, 20 mmol) and barbituric acid (2.56 g, 20 mmol) was refluxed in the presence of Et₃N (3.2 g, 32 mmol) in water–ethanol (15:15 mL) until a clear solution was obtained. The reaction was kept at reflux for an additional 2 h, then the solvent was removed by evaporation. After 2–3 days the resulting precipitate was washed several times with water and acetone, then dried. Red microcrystals with a yield of 80% and *T*_d = 245.49°C were obtained. MS *m/z*: 289 (M⁺), 258, 120. ¹H NMR δ: 10.73 (d, *J* = 11.46 Hz, 2H), 8.24 (d, *J* = 8.6 Hz, 2H), 7.98 (s, 1H), 6.68 (q, *J* = 8.6 Hz, 2H), 4.71 (1H, s), 3.53 (4H, s), 3.07 (3H, s). Element analysis: Anal. calcd.: C 58.12, H 5.23, N 14.53; found: C 57.64, H 4.85, N 14.38.

Crystal structure determination

Crystal data and other information on structure determination are given in Tables 2–4. X-ray diffraction data were made on a Bruker P4 four-cycle diffractometer and graphite-monochromated Mo Kα radiation was used ($\lambda = 0.71073$ Å). The structures were solved by direct method and refined by full-matrix least-squares on F^2 . The refinement was on F^2 of reflections with $F_0 \geq 4\sigma(F_0)$ to minimize $\sum w(|F_0| - |F_c|)^2$. Anisotropic displacement parameters were refined for all nonhydrogen atoms, and isotropic hydrogen atoms were constrained to ride on their parent carbon atoms with fixed bond lengths and idealized bond angles.

Linear optical property

The λ_{\max} values for all chromophores in DMF with $d_0 = 1.00 \times 10^{-5}$ M have been measured with a Hitachi U-3500

Table 4. Selected bond lengths (Å) and angles (°) for DPASPI.

C(1)—N(1)	1.481(16)	C(7)—C(8)	1.277(17)	C(17)—C(18)	1.360(17)
C(2)—N(1)	1.355(13)	C(8)—C(9)	1.427(16)	C(18)—C(19)	1.379(16)
C(6)—N(1)	1.320(15)	C(9)—C(14)	1.372(16)	C(19)—C(20)	1.362(16)
N(2)—C(12)	1.424(13)	C(9)—C(10)	1.431(16)	C(21)—C(22)	1.393(15)
N(2)—C(15)	1.416(13)	C(10)—C(11)	1.359(16)	C(21)—C(26)	1.387(60)
N(2)—C(21)	1.416(13)	C(11)—C(12)	1.381(15)	C(22)—C(23)	1.372(16)
C(2)—C(3)	1.359(16)	C(12)—C(13)	1.393(15)	C(23)—C(24)	1.404(19)
C(3)—C(4)	1.353(17)	C(13)—C(14)	1.375(16)	C(24)—C(25)	1.341(18)
C(4)—C(5)	1.412(19)	C(15)—C(16)	1.358(15)	C(25)—C(26)	1.359(16)
C(4)—C(7)	1.524(17)	C(15)—C(20)	1.425(15)		
C(5)—C(6)	1.388(17)	C(16)—C(17)	1.377(16)		
C(1)-N(1)-C(2)	117.6(9)	C(8)-C(9)-C(10)	126.2(10)	C(17)-C(18)-(19)	118.7(11)
C(1)-N(1)-C(6)	123.4(9)	C(8)-C(9)-C(14)	118.2(10)	C(18)-C(19)-(20)	122.8(11)
C(2)-N(1)-C(6)	118.8(8)	C(10)-C(9)-C(14)	115.6(10)	C(15)-C(20)-(19)	117.5(10)
C(12)-N(2)-C(15)	119.9(8)	C(9)-C(10)-C(11)	120.9(11)	N(2)-C(21)-(22)	121.1(10)
C(12)-N(2)-C(21)	116.8(8)	C(10)-C(11)-C(12)	122.0(10)	N(2)-C(21)-(26)	121.3(9)
C(15)-N(2)-C(21)	122.6(8)	N(2)-C(12)-C(11)	123.5(9)	C(22)-C(21)-(26)	117.5(10)
N(1)-C(2)-C(3)	121.6(8)	N(2)-C(12)-C(13)	118.5(9)	C(21)-C(22)-(23)	121.9(11)
C(2)-C(3)-C(4)	121.9(11)	C(11)-C(12)-C(13)	118.1(10)	C(22)-C(23)-(24)	117.8(11)
C(3)-C(4)-C(5)	116.3(11)	C(12)-C(13)-C(14)	119.6(10)	C(23)-C(24)-(25)	120.9(12)
C(3)-C(4)-C(7)	118.7(11)	C(9)-C(14)-C(13)	123.7(11)	C(24)-C(25)-(26)	120.8(11)
C(5)-C(4)-C(7)	125.0(11)	N(2)-C(15)-C(16)	121.7(9)	C(21)-C(26)-(25)	121.1(10)
C(4)-C(5)-C(6)	119.8(11)	N(2)-C(15)-C(20)	119.0(9)	C(16)-C(17)-(18)	120.4(10)
N(1)-C(6)-C(5)	121.6(11)	C(16)-C(15)-C(20)	119.2(10)	C(15)-C(16)-(17)	121.3(10)
C(4)-C(7)-C(8)	124.5(12)	C(7)-C(8)-C(9)	123.7(12)		

Linear optical property

The λ_{\max} values for all chromophores in DMF with $d_0 = 1.00 \times 10^{-5}$ M have been measured with a Hitachi U-3500 recording spectrophotometer from quartz cuvettes of 1 cm path.

Measurement of the two-photon absorption cross section (δ value)

The Z-scan system with an open aperture ($S = 1$), which is insensitive to the nonlinear refraction, can be used to measure the nonlinear absorption cross-section. Such Z-scan traces with open apertures are expected to be symmetrical with respect to the focus ($Z = 0$), where they have a minimum transmittance (e.g., multiphoton absorption) or a maximum transmittance (e.g., saturation of absorption). In fact, the nonlinear absorption coefficient (β) that is due to TPA can be easily calculated from the transmittance curves.

For a temporally Gaussian pulse, the normalized energy transmittance can be given as (19),

$$[3] \quad T(z, S = 1) = \frac{1}{\sqrt{\pi}q_0(z,0)} \int_{-\infty}^{+\infty} \ln(1 + q_0)(z,0) e^{-\tau^2} d\tau$$

where $q_0(z,t) = \beta I_0 L_{\text{eff}} / (1 + z^2/z_0^2)$. When there is no linear absorption, $L_{\text{eff}} = L$. L is the sample thickness, z_0 and $\pm z$ are the position of focus point and the range of scanning, respectively, and I_0 is the peak irradiance.

For $|q_0| \ll 1$, the transmittance (T) can be expressed in terms of the peak irradiance in a summation form more suitable for numerical evaluation,

$$[4] \quad T(z, S = 1) = \sum_{m=0}^{\infty} \frac{[-q_0(z,0)]^m}{(m+1)^{3/2}} = \sum_m \frac{\beta I_0 L / (1 + z^2/z_0^2)}{(m+1)^{3/2}}$$

Thus, once an open-aperture Z-Scan ($S = 1$) is performed, the TPA coefficient β can be unambiguously deduced and if the concentration d_0 (in units of mol L⁻¹) of the solution is known, the molecular TPA cross section δ (in units of cm⁴ s per photon) can be determined by using the following relationship,

$$[5] \quad hv\beta = \delta N_A d_0 = hv\delta N_A d_0 \times 10^{-3}$$

where hv is the energy of the incident photon. N_A is Avogadro's constant.

We have accomplished TPA cross-section measurement for all chromophores with the sample thickness of 2 mm and a relatively high concentration of $d_0 = 0.05$ M, using a focussed 35 ps, 1064 nm mode-locked Nd:YAG laser. Using the above equations, we can get the TPA coefficient (β) and TPA δ value, which are presented in Table 1. The final measured results of all samples are given in Table 1 with an experimental uncertainty of $\pm 15\%$. The typical open aperture Z-scan curves are shown in Fig. 1, which depicts the open-aperture trace at peak irradiance $I_0 = 3.64$ GW cm⁻².

Calculation of the structures

Charge density distribution in both ground and excited states, the difference between the ground and excited state dipole moment ($\Delta\mu_{ge}$), the transition dipole moment between two lowest states ($M_{ee'}$), and the dihedral angle between two rings of the backbone ($\theta^{d/0}$) were all calculated with the PM3 and ZINDO semiempirical methods.

Fig. 1. Normalized Z-scan transmittance of: (a) DPASQI and (b) HMASQI, measured using ps pulses at $\lambda = 1064$ nm with $I_0 = 3.64$ GW cm⁻².

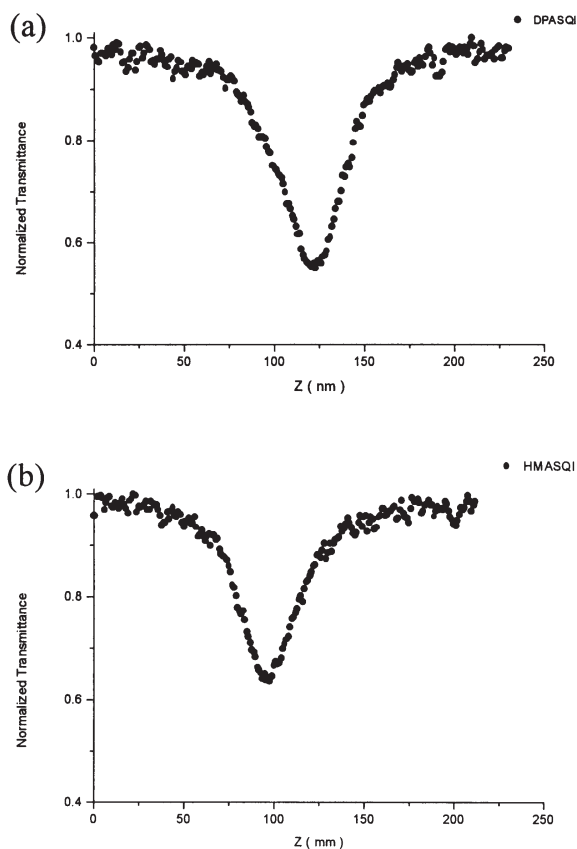
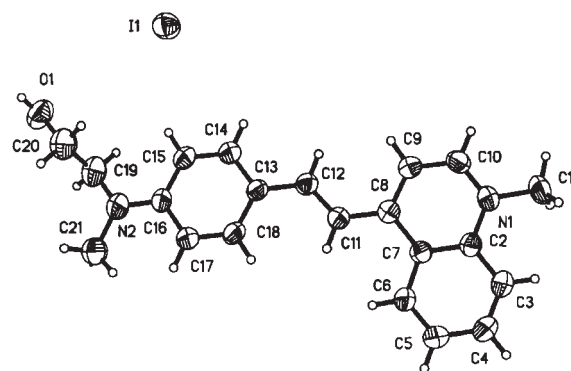


Fig. 2. Molecular structure of HMASQI.



monoclinic crystal system of the centrosymmetric space group $P2_1/n$ with the unit cell parameters of $a = 10.0512(11)$ Å, $b = 16.2879(12)$ Å, $c = 12.3328(8)$ Å, $\beta = 102.307(6)^\circ$. Bond lengths of C8—11, C11—12, and C12—13 are 1.436(5), 1.352(5), and 1.442(5) Å, respectively owing to strong π -electron conjugation between the substituted phenyl ring and quinolinium ring. Bond angles of $\angle C6-7-8$, $\angle C2-7-8$, $\angle N1-C2-C3$, and $\angle N1-C2-C7$ are $122.4(4)^\circ$, $120.3(3)^\circ$, $120.4(4)^\circ$, and $119.2(3)^\circ$, respectively, which shows that the quinolinium ring possesses excellent planarity. The packing diagram shows that HMASQI molecules stack to form a layer-like structure along the b -axis. The donor-end of one

Fig. 3. Packing diagram of HMASQI.

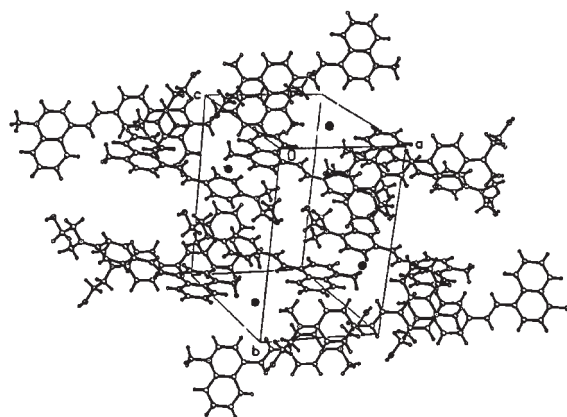
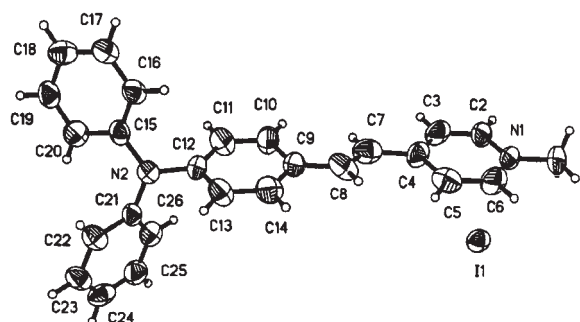


Fig. 4. Molecular structure of DPASQI.

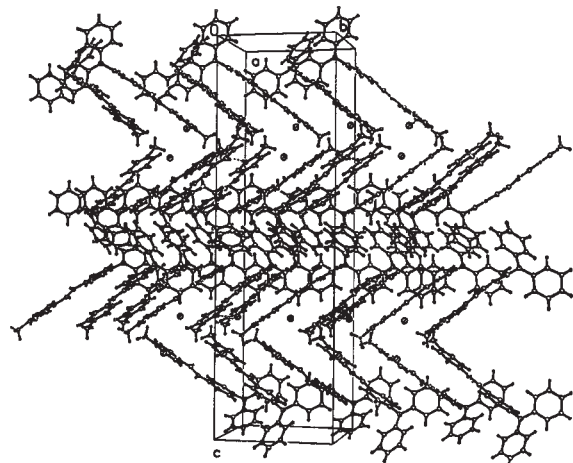


molecule is overlapped with the acceptor-end of the other molecule along the a -axis. The anions (I^-) fill in the space among the cations.

The structures of DPASQI are shown in Figs. 4 and 5. This crystal belongs to the orthorhombic crystal system of centrosymmetric space group $Pbca$ with eight molecules in the unit cell. The two phenyl rings of the backbone are almost in the identical plane with the dihedral angle of 3.6° , while the other two phenyl rings on the donor-end deviate from this plane. From the packing diagram of DPASQI (shown in Fig. 5), one can see that the donor groups overlap, or stagger, each other while the acceptor-ends align face to face with the definite degree. Along the c -axis, the donor- and acceptor-groups present chain-like channels among the space filling in the anions.

Two-photon absorption and intramolecular charge transfer

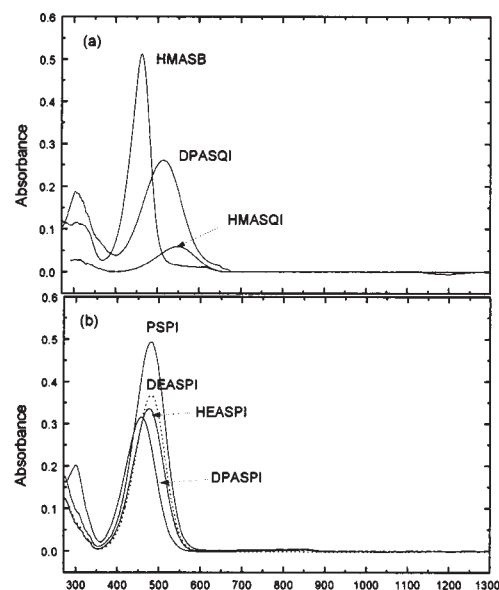
Linear absorption for all chromophores is shown in Fig. 6. The influences from the quartz liquid cell and the solvent DMF have been subtracted. One can see that maximum absorption bands are 463 nm for the barbituric acid derivative and 458 ~ 482 nm for the pyridinium derivatives. Upon replacing the acceptor group with a larger conjugated fragment (N -methyl-quinolinium) one can observe a bathochromic shift of the long-wave absorption band to 514 ~ 554 nm. This suggests that the electronic interactions between the donor and acceptor groups induce the spectral shift to lower energy in the order of: quinolinium derivatives > pyridinium derivatives > barbituric acid derivatives.

Fig. 5. Packing diagram of DPASPI.

It must be noted that there is no linear absorption for all chromophores in the region from ~ 700 to ~ 1300 nm. So pumped by a 1064 nm laser pulse, the linear absorption can be excluded because two-photon excitation via virtual intermediate state can proceed, consistent with the fact that the nonlinear absorption occurs at a frequency in the region of one-photon transparency. It should be stressed that valid structure–property relationships can only be ascertained for those molecules that have their two-photon absorption peak at approximately the same wavelength. If the two-photon absorption peak shifts greatly from the wavelength that is away from the experimental wavelength of 1064 nm, then the comparison of absolute cross-sections is misleading. From Fig. 6, one can see that the maximum absorption wavelengths of all chromophores do not deviate too much. It is for this reason that the structure–property relationships deduced from the experimental data in this work are valid at 1064 nm.

Two-photon absorption cross-sections measured in DMF for the newly synthesized chromophores are summarized in Table 1. From Table 1, one can see that when the acceptor is fixed to the *N*-methyl pyridinium moiety, while the donor strength decreases, the δ values increase from 5.7×10^{-48} cm⁴ s per photon for PSPI, to 7.0×10^{-48} cm⁴ s per photon for HEASPI, to 8.8×10^{-48} cm⁴ s per photon for DPASPI. This suggests that the δ value is not always proportional to the donor strength. Similar results can be observed in quinolinium moiety. When acceptor is fixed to *N*-methyl quinolinium moiety, with the decrease in donor strength, the two-photon absorption cross-section values change from 8.8×10^{-48} cm⁴ s per photon for HMASQI to 10.9×10^{-48} cm⁴ s per photon for DPASQI.

It is clear that with the acceptor structural factor changing from barbituric acid to pyridinium and further to quinolinium, δ values are gradually enhanced, in the range of $3.8 \times 10^{-48} \sim 10.9 \times 10^{-48}$ cm⁴ s per photon. The barbituric acid derivative exhibits a relatively small cross-section, which can be explained as the molecular planarity seems to be critical in enhancing TPA cross-section values. Calculation shows that the dihedral angle between the benzene ring and the barbituric acid (70° for HMASBA) distorts the planarity and reduces the conjugated length, which is a disadvantage with respect to intramolecular charge transfer.

Fig. 6. Vis-IR absorption spectra of all chromophores in DMF with $d_0 = 1.00 \times 10^{-5}$ M.

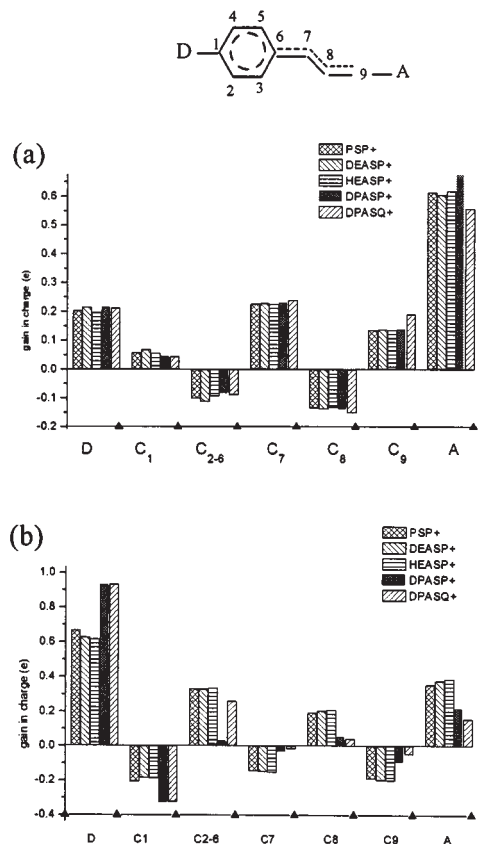
Replacing barbituric acid by a pyridinium or a quinolinium fragment, greatly decreases the dihedral angle between two aromatic rings so as to be negligible. Consequently, a relatively large value for the cross-section was obtained.

In a comparison of these newly synthesized compounds with some other chromophores recently reported (13, 20), we found that the δ value of 10.9×10^{-48} cm⁴ s per photon for DPASQI is remarkable considering the limited conjugation length. For example, the TPA δ value for DPASQI is nearly same as that of 6-(4-pyridyl)-*N,N*-diphenyl-2-naphthylamine ($\delta = 12.9 \times 10^{-48}$ cm⁴ s per photon) (13), but almost twice that of the nitro-containing fluorescent derivative ($\delta = 6.5 \times 10^{-48}$ cm⁴ s per photon) (20). The difference of their TPA cross-section resulting from the variation of both the acceptor group and the character of the conjugated bridge shows that the quinolinium ring is a good acceptor group and that the TPA δ value can be significantly enhanced if a better planar moiety (as a conjugated bridge) is inserted in a donor-quinolinium ring pair. Since the quinolinium ring possesses better planarity, as confirmed by the crystallographic data of HEASQI mentioned above, this characteristic has to contribute to the intramolecular charge transfer that can be measured by such structural parameters as $\Delta\mu_{ge}$ and $M_{ee'}$ or the change of charge distribution on each atom between the ground and the excited state.

The structural parameters calculated by the PM3 and ZINDO methods are presented in Table 1. From this table, one can conclude that the chromophores with large $\Delta\mu_{ge}$ and $M_{ee'}$ values possess relatively high δ value. For example, $M_{ee'}$ values in pyridinium derivatives change in the order of $DPASP^+ > HEASP^+ \sim PSP^+ \sim DEASP^+$, while $\Delta\mu_{ge}$ values change in the order of $DPASP^+ > HEASP^+ \sim DEASP^+ \gg PSP^+$. The measured δ values, with the order of $DPASPI > HEASPI \sim DEASPI > PSPI$, confirmed that the experimental results are in agreement with the calculation.

Charge density (e) distribution for part of the chromophore cations in the ground state (shown in Fig. 7(a)), and in the

Fig. 7. Histogram of the π -charge distribution (e) in the: (a) ground state and (b) in the excited state, for part of the chromophores.



excited state (shown in Fig. 7(b)), are plotted in histogram form. One can see that in the ground state there is no alternation of charge density distribution. For example, the charge densities over D (donor) and atom C1 are both positive, and the charge densities over A (acceptor) and atom C9 are both positive too. Once in the excited state, the great charge redistribution occurs, accompanying with the significant charge positive–negative alternation, where the positive charge increases on the donor-end (D), and in the meantime, decreases on the acceptor-end (A). For example, one can see that in the ground state, the charge distribution of the DPASP⁺ cation is in such a way: $Q_D = +0.21$ e and $Q_A = +0.83$ e; while in the excited state, $Q_D = +0.93$ e and $Q_A = +0.21$ e, indicating a large charge redistribution on the two-terminals occurs. It is interesting to note that such a π -charge transfer degree is consistent with the $\Delta\mu_{ge}$ and $M_{ee'}$ values and also in accordance with the enhancement of δ value. So DPASPI exhibits relatively large δ values among pyridinium derivatives because of its larger $\Delta\mu_{ge}$ (11.8 debye) and $M_{ee'}$ (9.8 debye) values. HMASBA exhibits smaller δ value because of its small change of dipole moment (0.8 debye). Its charge distribution is also small: $Q_{ami} = +0.04$ e, $Q_{bar} = -0.27$ e in the ground state, and $Q_{ami} = +0.25$ e, $Q_{bar} = -0.28$ e in the excited state, which shows that only a weak charge transfer between the ground and the excited state has occurred.

Conclusions

A series of new chromophores, styryl-parent end-capped with various substituted amino groups as donors, and barbituric acid, methyl-pyridinium, and methyl-quinolinium as the acceptors, has been synthesized and characterized by element analysis or X-ray diffraction.

We confirm both theoretically and experimentally that the TPA cross-section is strongly influenced by intramolecular charge transfer, which is characterized by the difference between the ground and excited state dipole moment ($\Delta\mu_{ge}$) and the transition dipole moment between the excited states ($M_{ee'}$) or the change of charge distribution on each atom between ground and excited state. Based on above point of view, the structure–property relationships of two-photon absorption (TPA) property can be interpreted reasonably, which can provide some useful information for molecular design with large TPA cross-sections.

The barbituric acid derivative possesses a relatively small TPA cross-section value due to its being heavily distorted from planarity and short conjugated length, which hinders intramolecular charge transfer. In contrast to this, quinolinium derivatives exhibit relatively large TPA cross-section due to its excellent planarity.

Both the *N,N*-diphenylamino group and the quinolinium ring are effective groups for enhancing TPA cross-sections, although the *N,N*-diphenylamino group is not a strong donor in comparison with the *N,N*-diakylamino group. Quantum chemical calculation shows that when the *N,N*-diphenylamino group and the quinolinium ring are matched, a relatively large charge transfer is produced ($\Delta\mu_{ge} = 12.1$ debye), which confirms that TPA cross-section is not proportional to electron-donating strength, but dominated by intramolecular charge transfer.

Acknowledgments

This work was supported by a grant for State program of China. The authors are grateful to Prof. Sun Zhenrong and Prof. Ding Liangen in the Department of Physics, Normal University of East China for their help to measure the two-photon absorption cross-sections for all chromophores.

References

1. B.H. Cumpston, S.P. Ananthavel, and S. Barlow. *Nature* (London), **3**, 1041 (1999).
2. D.A. Parthenopoulos and P.M. Rentzepis. *J. Appl. Phys.* **68**, 5814 (1990).
3. D.A. Parthenopoulos and P.M. Rentzepis. *Science* (Washington, D.C.), **245**, 843 (1989).
4. J.E. Ehrlich, X.L. Wu, and I.Y.S. Lee. *Opt. Lett.* **22**, 1843 (1997).
5. G.S. He, R. Gvishi, P.N. Prasad, and B.A. Reinhardt. *Opt. Commun.* **117**, 133 (1995).
6. G.S. He, R. Signorini, and P.N. Prasad. *Appl. Opt.* **37**, 5720 (1998).
7. J.D. Bhawalkar, G.S. He, and P.N. Prasad. *Rep. Prog. Phys.* **59**, 1052 (1996).
8. G.S. He, L. Yuan, and Y.P. Cui, M. Li, and P.N. Prasad. *J. Appl. Phys.* **81**, 2529 (1997).

9. G.S. He, K.S. Kim, L.X. Yuan, N. Cheng, and P.N. Prasad. *Appl. Phys. Lett.* **71**, 1619 (1997).
10. G.S. He, J.D. Bhawalkar, C.F. Zhao, C.K. Park, and P.N. Prasad. *Appl. Phys. Lett.* **68**, 3549 (1996).
11. C.F. Zhao, G.S. He, J.D. Bhawalkar, C.K. Park, and P.N. Prasad. *Chem. Mater.* **7**, 1979 (1995).
12. C.F. Zhao, C.K. Park, and P.N. Prasad. *Chem. Mater.* **7**, 1237 (1995).
13. B.A. Reinhardt, L.L. Brott, S.J. Clarson, A.G. Dillard, and J.C. Bhatt. *Chem. Mater.* **10**, 1863 (1998).
14. G.S. He, L.X. Yuan, N. Cheng, and P.N. Prasad. *J. Opt. Soc. Am. B*, **14**, 1079 (1997).
15. C.W. Spangler. *J. Mater. Chem.* **9**, 2013 (1999).
16. M. Albota, D. Beljonne, J.L. Bras, J.E. Ehrlich, J.Y. Fu, A.A. Heikal, and S.E. Hess. *Science (Washington, D.C.)*, **281**, 11 (1998).
17. F. Meyers, S.R. Marder, B.M. Pierce, and J.L. Brédas. *J. Am. Chem. Soc.* **116**, 10 703 (1994).
18. T. Kogej, D. Beljonne, F. Meyyers, J.W. Perry, S.R. Marder, and J.L. Brédas. *Chem. Phys. Lett.* **298**, 1 (1998).
19. S.B. Mansoor, A.A. Said, T.H. Wei, D.J. Hagan, and E.W.V. Stryland. *IEEE J. Quantum Electron.* **26**, 760 (1990).
20. K.D. Belfield, D.J. Hagan, E.W.V. Stryland, K.J. Schafer, and R.A. Negres. *Org. Lett.* **1**, 10 (1999).